Enhanced Long-Distance Weak Signal Transmission Capabilities via Weak Measurement

Ding Wang(王丁)[1†], Qi Song(宋琦)[1†], Hongjing Li(李洪婧)[1,2,3*], Zhiqiang Liu(刘志强)[1], Jingzheng Huang(黄靖正)[1,2,3], and Guihua Zeng(曾贵华)[1,2,3]

[1]*State Key Laboratory of Photonics and Communications, Institute for Quantum Sensing and Information Processing, School of Sensing Science and Engineering, Shanghai Jiao Tong University, Shanghai 200240, China*
[2]*Hefei National Laboratory, Hefei 230088, China*
[3]*Shanghai Research Center for Quantum Sciences, Shanghai 201315, China*

(Received 12 May 2025; accepted manuscript online 19 September 2025)

Reliable detection of weak phase signals under significant channel loss and complex noise environments is a crucial step for practical applications of optical integrated communication and sensing systems. In this letter, we propose and experimentally demonstrate an enhanced long-distance weak signal transmission method assisted by weak measurement. Performing heterodyne detection and light intensity compensation on two nearly symmetric post-selected paths, the method enables real-time estimation of a time-varying phase while maintaining robustness against technical noises proportional to light intensity or photon number, detector common-mode noise, and significant attenuation over long-distance transmission. Experimental results indicate a potential phase sensitivity at the level of 10^{-8} rad even with a signal light intensity attenuation of 48.1 dB. Potentially, combining the adaptive adjustment strategy, the method may provide a viable solution in remote weak signal detection and extraction, thereby contributing to optical integrated communication and sensing.

DOI: 10.1088/0256-307X/42/11/110402 CSTR: 32039.14.0256-307X.42.11.110402

Integrated communication and sensing is capable of performing additional sensing tasks in long-distance communication, which has attracted considerable attention in application scenarios such as environmental monitoring,[1,2] smart home,[3–6] and internet of vehicles.[7–9] Optical-integrated communication and sensing (O-ICAS), benefiting from outstanding monochromaticity and coherence, wide bandwidth, and small divergence angle of light beam, offers high-rate communication, higher resolution, and finer environmental information compared to radio-frequency integrated communication and sensing, with implementations in both quantum[10,11] and classical[12–14] platforms. The information in O-ICAS systems can be encoded through modulating the intensity, frequency, or phase of light beam. In typical implementations, encoding transmission signals as the phase parameter improves signal correlation, security, and anti-noise performance.[15,16] However, long-distance transmission between the signal sensing unit and the signal processing unit is usually required in O-ICAS system, which leads to significant attenuation. Additionally, adverse factors such as source fluctuation, channel noise, and phase-recovery noise may completely overwhelm weak phase signals,[17–20] imposing higher demands on the receiver. Weak measurement provides a promising approach for amplifying weak phase signals beyond the limitations of technical noise, thereby significantly enhancing the signal-to-noise ratio (SNR).[21–24] In 2010, Brunner and Simon demonstrated that weak measurement could outperform conventional interferometry by over three orders of magnitude in phase measurement.[25] Following this breakthrough, weak-measurement-based phase sensing has garnered extensive research attention, leading to the development of various refined methods, including standard weak measurement,[26] joint weak measurement,[27–29] biased weak measurement,[30] and dual weak measurement.[31] However, these methods typically rely on spectral detection techniques, and long integration time inherently restricts the achievable signal sampling rates, posing a challenge for real-time monitoring of time-varying signals. While recent advances have introduced light intensity detection as a viable alternative,[32–34] the accompanying intensity attenuation remains a practical concern, particularly in applications requiring long-distance signal transmission.

In this Letter, an enhanced long-distance weak signal transmission method via weak measurement is proposed that can realize accurate estimation of weak time-varying phase signals at a light intensity of −80 dBm. Leveraging heterodyne detection, the method can compensate for light intensity attenuation caused by near-orthogonal initial and post-selected states. Furthermore, introducing light intensity compensation eliminates the stringent requirements for symmetry in the two post-selection paths,

†These authors contributed equally to this work.
*Corresponding author. Email: lhjnet2012@sjtu.edu.cn
© 2025 Chinese Physical Society and IOP Publishing Ltd. All rights, including for text and data mining, AI training, and similar technologies, are reserved.

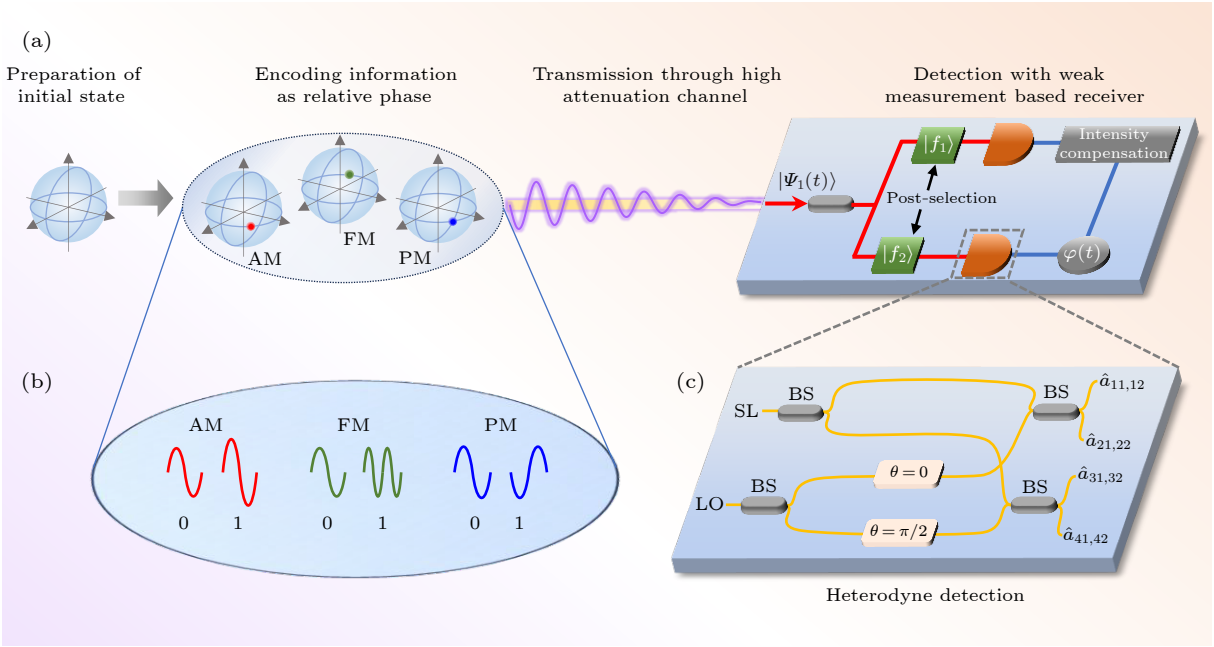

Fig. 1. Conceptual model of the enhanced long-distance weak signal transmission method via weak measurement. (a) Theoretical model. (b) Information encoding modulation scheme. (c) Schematic diagram of heterodyne detection. The abbreviations in the figure are as follows: AM: amplitude modulation, FM: frequency modulation, PM: phase modulation, SL: signal light, LO: local oscillator light.

facilitating real-time estimation of the weak time-varying phase signal while maintaining robustness against technical noises proportional to light intensity or photon number and detector common-mode noise. Experimental results demonstrate that the proposed method can accurately estimate weak communication signals even with a 48.1 dB attenuation in the signal light, which guarantees the realizability for above performance in long-distance transmission.

A weak measurement enhanced method for long-distance weak signal transmission is proposed, mainly involving encoding signals as relative phases on the light field or quantum states and a weak-measurement-based receiver, as illustrated in Fig. 1(a). The procedure can be broken down into four stages: preparation of the initial state, encoding information as relative phase, transmission through a high-attenuation channel, and detection utilizing a weak-measurement-based receiver.

In the preparation of the initial state, we consider the coherent state $|\alpha\rangle$ as the probe light, where $\alpha = x + \mathrm{i}p$, x and p are regular components, and the mean photon number is $|\alpha|^2$. The initial state is modulated as $|i\rangle = 1/\sqrt{2}(|H\rangle + |V\rangle)$, where $|H\rangle$ and $|V\rangle$ are horizontal and vertical polarization states, respectively. During the encoding process, the information to be transmitted is encoded on the relative phase of the pointer polarization; in this case, the observable operator can be defined as $\hat{A} = |H\rangle\langle H| - |V\rangle\langle V|$. Signals of interest are encoded as a tiny time-varying phase shift $|\varphi(t)| \ll 1$, and the process can be described by a unitary evolution $\hat{U}(t) = \mathrm{e}^{-\mathrm{i}\hat{A}\varphi(t)/2}$. Typically, amplitude modulation (AM), frequency modulation (FM), and phase modulation (PM) are three fundamental modulation methods in communication systems that are used to encode baseband signals onto carrier signals for signal transmission. Without loss of generality, binary coding is taken as an example, where "0" corresponds to low amplitude in AM, low frequency in FM, and an initial phase of 0 in PM, while "1" represents high amplitude, high frequency, and initial phase of π, respectively, as depicted in Fig. 1(b). It is worth noting that these modulation methods can be utilized either individually or in combination.

After transmitting through a long-distance channel with high attenuation, denoted by the attenuation coefficient in the channel as η, the evolved state $|\Psi_1(t)\rangle$ is collected by the weak-measurement-based receiver. The evolved state is projected on two symmetrical post-selected states, i.e., $|f_{1,2}\rangle = \frac{1}{\sqrt{2}}(\mathrm{i}\mathrm{e}^{\pm\mathrm{i}\varepsilon}|H\rangle - \mathrm{i}\mathrm{e}^{\mp\mathrm{i}\varepsilon}|V\rangle)$, where $0 < \varepsilon \ll 1$ is the post-selection angle. The combination of two post-selection states with the initial state leads to two weak values for the observable operator, i.e.,

$$Aw_{1,2} = \frac{\langle f_{1,2}|\hat{A}|i\rangle}{\langle f_{1,2}|i\rangle} = \pm\mathrm{i}\cot\varepsilon, \tag{1}$$

and we denote $\mathrm{Im}Aw = |\mathrm{Im}Aw_{1,2}| = \cot\varepsilon$. Correspondingly, the initial photon number of the system can be expressed as $N_i = \frac{1}{2}\eta|\langle f_1|i\rangle|^2|\alpha|^2 + \frac{1}{2}\eta|\langle f_2|i\rangle|^2|\alpha|^2$, which is attenuated by a factor of $\eta\sin^2\varepsilon$. To realize the real-time detection of time-varying signals, the received photon number is selected as the pointer.[34–36] Different from previous methods, heterodyne detection employing a local oscillator (LO) light with an amplitude of $|\alpha_{\mathrm{LO}}|$ is utilized to detect regular components, thereby obtaining the received photon number in the detection, as illustrated in Fig. 1(c). With each detection value, regular components can be retrieved, i.e., $x_{1,2} = \hat{a}^\dagger_{11,12}\hat{a}_{11,12} - \hat{a}^\dagger_{21,22}\hat{a}_{21,22}$ and $p_{1,2} = \hat{a}^\dagger_{31,32}\hat{a}_{31,32} - \hat{a}^\dagger_{41,42}\hat{a}_{41,42}$, where $\hat{a}_{11,12}, \hat{a}_{21,22}, \hat{a}_{31,32}$, and

$\hat{a}_{41,42}$ are the annihilation operators corresponding to output optical modes of heterodyne detection, respectively, and the superscript "†" means the corresponding creation operator. The received photon number can be given by $N_{1,2}(t) = x_{1,2}^2 + p_{1,2}^2 = \frac{1}{2}\eta|\alpha_{\rm LO}|^2|\alpha|^2|\langle f_{1,2}|\hat{U(t)}|i\rangle|^2$, and especially within the range of $|\varphi(t)/2 \cdot {\rm Im}Aw| \ll 1$,[37,38] the photon number of two paths can be rewritten as

$$N_{1,2}(t) \approx \frac{1}{2}\eta|\alpha_{\rm LO}|^2|\alpha|^2|\langle f_{1,2}|i\rangle|^2\{1 \pm \sin[\varphi(t){\rm Im}Aw]\}. \quad (2)$$

Subsequently, the modified received photon number can be calculated by

$$N_1(t) - N_2(t) \approx \eta|\alpha_{\rm LO}|^2|\alpha|^2\sin^2\varepsilon\sin[\varphi(t){\rm Im}Aw]. \quad (3)$$

As illustrated by the blue line in Fig. 2(a), the method yields a linear dynamic range on the tiny phase shift, and $\varphi(t)$ can be retrieved as

$$\varphi(t) \approx \frac{N_1(t) - N_2(t)}{\eta|\alpha_{\rm LO}|^2|\alpha|^2{\rm Im}Aw\sin^2\varepsilon}. \quad (4)$$

Indeed, the phase shift can also be retrieved by employing a single post-selected detection path, i.e., $N_1(t)$ or $N_2(t)$,[33,36] but an error emerges in the linear dynamic range due to the asymmetry near $\varphi(t) = 0$. Although the error can theoretically be eliminated via calibration, the actual measurement precision is affected due to the additional offset. With symmetrical post-selected detection paths, $\varphi(t)$ exhibits a symmetrical linear dynamic range without offset. Meanwhile, common-mode noise can be effectively suppressed by $N_1(t) - N_2(t)$, which is beneficial for practical detection.

However, the asymmetry of the two post-selected detection paths may lead to errors in the retrieved value, and the detection values can be expressed as $N_{1,2}^{\rm R}(t) = \eta\eta_{1,2}|\alpha_{\rm LO}|^2|\alpha|^2\sin^2(\pm\varepsilon + \Delta\varepsilon_{1,2})(1 + \varphi(t){\rm Im}Aw_{1,2})$ with ${\rm Im}Aw_1 = \cot(\varepsilon+\Delta\varepsilon_1)$ and ${\rm Im}Aw_2 = \cot(-\varepsilon+\Delta\varepsilon_2)$, where $\Delta\varepsilon_{1,2}$ represent the errors in post-selection angles, and $\eta_{1,2}$ represent the light intensity attenuation coefficients for the two post-selected detection paths, respectively, which may arise from non-ideal characteristics such as differences in the transmission of optical devices within each path. To evaluate the performance of the proposed method, the relative change between the modified received and the initial photon numbers is chosen as the performance metric. Under the ideal conditions, the relative change can be given by

$$C_i(t) = \frac{N_1(t) - N_2(t)}{N_i} \approx |\alpha_{\rm LO}|^2\sin[{\rm Im}Aw\varphi(t)], \quad (5)$$

which indicates that the phase shift is amplified by ${\rm Im}Aw$, and the application of heterodyne detection introduces an additional gain factor of $|\alpha_{\rm LO}|^2$ on the received photon number. When asymmetry of two post-selected paths occurs in the system, the relative change can be expressed as

$$\begin{aligned} C_{\rm N}(t) &= \frac{N_1^{\rm R}(t) - N_2^{\rm R}(t)}{N_i} \\ &\approx |\alpha_{\rm LO}|^2\Big\{\frac{\eta_1\sin^2(\varepsilon+\Delta\varepsilon_1) - \eta_2\sin^2(-\varepsilon+\Delta\varepsilon_2)}{\sin^2\varepsilon} \\ &\quad + ({\rm Im}Aw)\varphi(t) \\ &\quad + \frac{\cos 2\varepsilon[\eta_1\sin(2\Delta\varepsilon_1) - \eta_2\sin(2\Delta\varepsilon_2)]}{2\sin^2\varepsilon}\varphi(t)\Big\}, \end{aligned} \quad (6)$$

which indicates that a bias is introduced and the amplification factor has an error. Consequently, the advantage of symmetry is lost, and the optical path design becomes more complex compared to the single post-selected detection path. Therefore, intensity compensation is performed on $N_1(t)$ with a compensation factor of $\gamma = \frac{\eta_2\sin^2(-\varepsilon+\Delta\varepsilon_2)}{\eta_1\sin^2(\varepsilon+\Delta\varepsilon_1)}$. The essence of intensity compensation is the correction of light intensity, which can be achieved through data processing or adjusting the optical devices in the experiment. Given that the two LO intensities are theoretically designed to be equal, any experimental deviation in LO light intensities will require a corresponding proportional adjustment to γ. After compensation, the relative change can be further expressed as

$$\begin{aligned} C(t) &= \frac{\gamma N_1^{\rm R}(t) - N_2^{\rm R}(t)}{\gamma\eta\eta_1|\alpha|^2\sin^2(\varepsilon+\Delta\varepsilon_1) + \eta\eta_2|\alpha|^2\sin^2(-\varepsilon+\Delta\varepsilon_2)} \\ &\approx |\alpha_{\rm LO}|^2\frac{{\rm Im}Aw_1 - {\rm Im}Aw_2}{2}\varphi(t). \end{aligned} \quad (7)$$

As depicted by the yellow and red dashed lines in Fig. 2(a), the additional offset can be eliminated, and the amplification factor will change from $|\alpha_{\rm LO}|^2{\rm Im}Aw$ to $|\alpha_{\rm LO}|^2({\rm Im}Aw_1 - {\rm Im}Aw_2)/2$, which has little effect on the retrieved $\varphi(t)$ with calibration.

In practice applications, the system encounters from some technical issues.[25,33,34,36] Here, we consider two types: one of which is the noise proportional to the light intensity or photon number, such as relative intensity noise and thermal noise, while the other is significant intensity attenuation during long-distance transmission. To illustrate the advantages of the proposed method, a comparative analysis is conducted with standard interference technique and previous weak measurement method with two symmetrical post-selected paths. For the standard interference technique, an equivalent standard interferometer (ESI) described by Bruner and Simon[25] is designed, where the probe light is polarized by $|i\rangle$; it also introduces a tiny time-varying phase shift $|\varphi(t)| \ll 1$ between $|H\rangle$ and $|V\rangle$ and subsequently projected onto $1/\sqrt{2}(|H\rangle \pm {\rm i}|V\rangle)$. Correspondingly, the phase shift can be retrieved with $I_1^{\rm ESI} - I_2^{\rm ESI} = \eta I_0\varphi(t)$, where I_0 is the initial light intensity of the source. For previous weak measurement method, adaptive weak measurement (AWM) in our recent work[32] without reference phases is adopted, where the pre-selection, weak interaction, and post-selection states are also $|i\rangle$, $\hat{U}(t)$, and $|f_{1,2}\rangle$, respectively, while the phase shift can be retrieved by $I_1^{\rm AWM} - I_2^{\rm AWM} = \eta I_0\sin^2\varepsilon({\rm Im}Aw)\varphi(t)$. Especially, the technical noise proportional to the light intensity or photon number can be expressed as $I_n = \chi I_0$ and $N_n = \chi N_0$, where χ denotes the noise coefficient. SNR is selected as the evaluation metric, which can be calculated as $R^{\rm ESI} \approx 20\lg[\varphi(t)/\chi]$ (dB) for ESI, and $R^{\rm AWM} \approx 20\lg[({\rm Im}Aw)\varphi(t)/\chi]$ (dB) for AWM. Assuming that the noise coefficients of signal light and LO light are identical in the proposed method, the SNR can be expressed as $R \approx 20\lg[({\rm Im}Aw)\varphi(t)/(\chi^2 + 2\chi)]$ (dB). The detailed derivation processes for these SNR calculations are provided in the "SNR analysis" of the Supplementary Materials (SM). From Fig. 2(b), SNR of proposed method

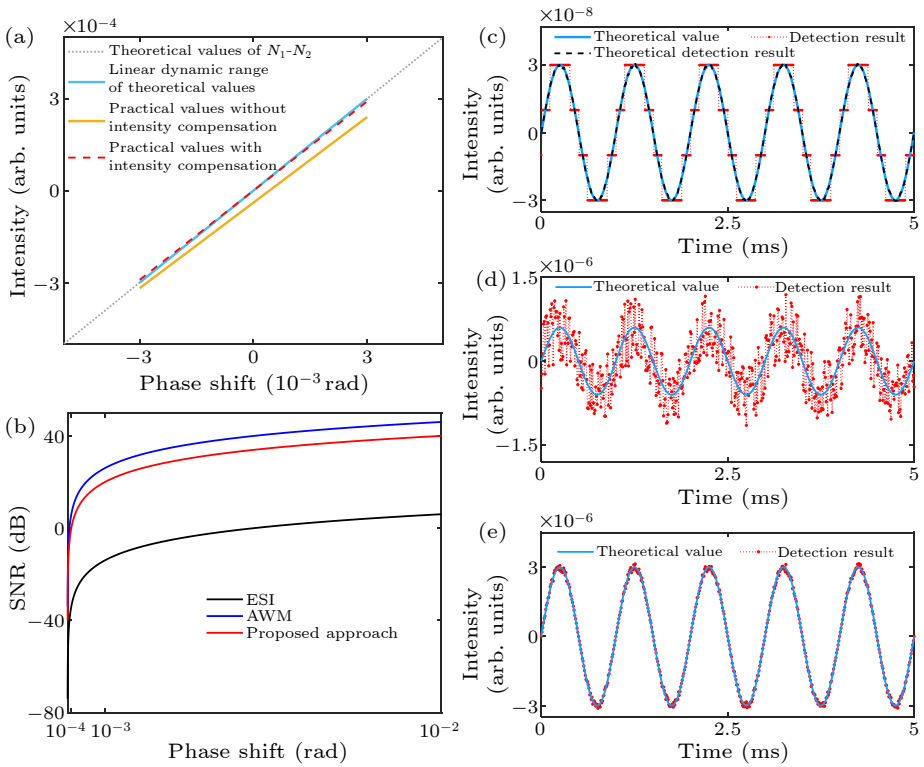

Fig. 2. (a) Performance analysis of light intensity compensation. The gray dot line represents the theoretical value of $N_1 - N_2$, while the blue, yellow, and red dash lines show the linear dynamic range of the theoretical value, the practical values with and without intensity compensation, respectively. Here, we set $\varepsilon = 0.01$. (b) Relationship between SNR for proposed method, ESI, and AWM under the influence of technical noise proportional to light intensity or photon number and varying phase shift. Simulation results of (c) AWM, (d) ESI, and (e) proposed method when suffering the significant intensity attenuation during long-distance transmission.

is $20\lg[(\chi^2+2\chi)/\chi]\,(\mathrm{dB}) \approx 6\,\mathrm{dB}$ lower than that of AWM but has an improvement factor about $\mathrm{Im}Aw$ than that of ESI; this improvement factor is determined by the post-selection angle and potentially achieves 4 orders of magnitude with a post-selection angle of $10^{-4}\,\mathrm{rad}$.

In the case of significant signal attenuation during long-distance transmission, the performance of AWM cannot be maintained as it is restricted by detection equipment. As depicted in Fig. 2(c), the detection results exhibit several discrete values, which prevent the retrieval of $\varphi(t)$, thereby degrading its performance below that of ESI depicted in Fig. 2(d). In contrast, the proposed method, as illustrated in Fig. 2(e), yields detection results that closely approximate the theoretical value, and its capability to suppress technical noise can be clearly observed. Although the SNR of proposed method is slightly lower compared to AWM, the response amplitude is enhanced by an additional factor of $|\alpha_{\mathrm{LO}}|^2$, which effectively avoids the influence of significant attenuation in long-distance transmission and demonstrates superior performance in suppressing technical noises proportional to light intensity or photon number.

To validate the feasibility of the proposed method, an experimental setup is designed, as shown in Fig. 3(a). The probe light emitted from a single-frequency laser is initially split into two paths. One path is further split into two paths to serve as the LO lights, while the other path is used as signal light, and attenuated by a variable optical attenuator (VOA) to simulate the intensity attenuation scenario encountered during long-distance transmission. In the preparation of the initial state, the light is polarized by a polarizer. During the weak interaction, a relative time-varying phase is generated via a phase modulator driven by an arbitrary waveform generator. In post-selection, the signal light is split into two paths and respectively post-selected by a quarter-wave plate and a polarizer. During detection, the signal light and the LO light pass through a hybrid and are detected by two balanced photodetectors in each path. Finally, the light intensities are recorded using a data acquisition card, and data processing is performed.

To systematically characterize the measurement performance, the detection response of time-varying phase shifts under different post-selection angles is initially investigated. In the experiment, a time-varying phase shift is generated by a phase modulator driven by an arbitrary waveform generator, where the driving output is a sinusoidal voltage with a frequency of 1 kHz and an amplitude of 100 mV, corresponding to a time-varying phase amplitude of approximately 14.28 mrad. Meanwhile, the received light intensity is attenuated to −80 dBm, which is lower than the minimum detectable power of the detector, making it challenging for previous weak measurement methods to effectively detect and amplify weak signals, as shown in Fig. 2(c). For the proposed method, through the application of heterodyne detection, intensity compensation and pre-calibrated experimental results, $\varphi(t)$ can be

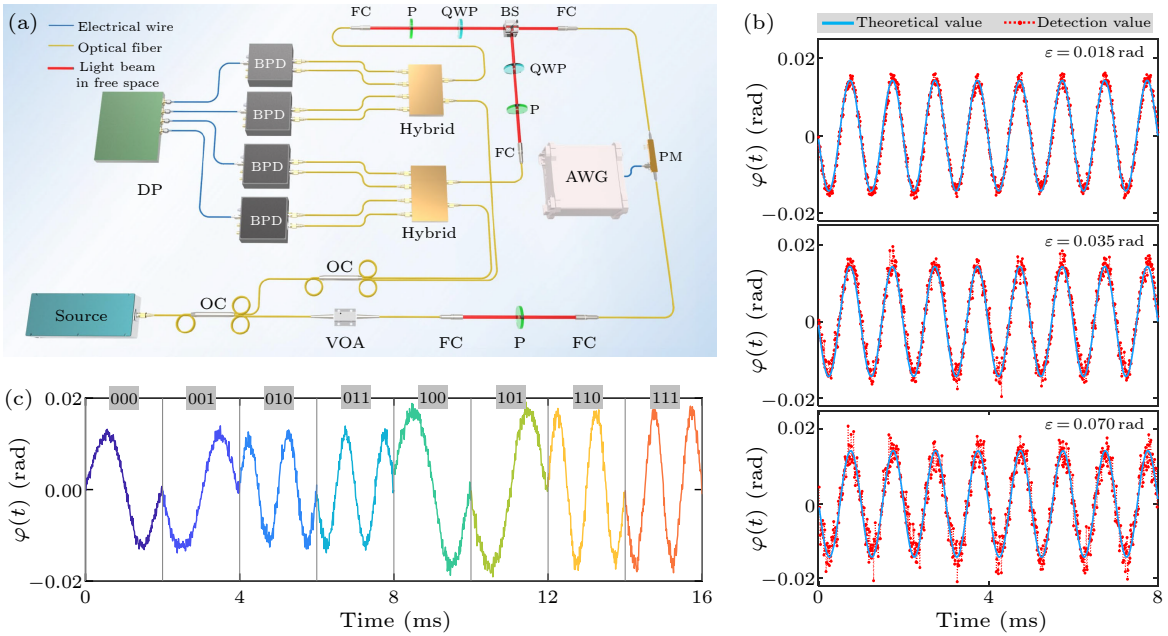

Fig. 3. (a) Schematic diagram of experimental setup. The yellow, red, and silver lines represent the optical fiber, light in free space, and electrical wire, respectively. The abbreviations in the figure are as follows: OC: optical coupler, VOA: variable optical attenuator, FC: fiber coupler, P: polarizer, PM: phase modulator, AWG: arbitrary waveform generator, BS: beam splitter, QWP: quarter-wave plate, BPD: balanced photodetector, DP data processing. (b) System performance analysis. Time-varying phase estimation with post-selection angles of 0.018, 0.035, and 0.07 rad, respectively. (c) Detection results for 3-bit binary coded communication signals, where first, second, and third bits modulate the initial phase, frequency, and amplitude, respectively. Here, the received light intensity is −80 dBm.

retrieved well, as illustrated in Fig. 3(b). It is important to emphasize that two signal light intensities in the experiment are consistent by adjusting fiber couplers prior to each adjustment of the post-selection angle and subsequent execution of experiments; and that LO light intensities feeding into the hybrids are measured as 0 dBm and −0.039 dBm, resulting in $\gamma = 0.991$. The detection results of the proposed method agree well with theoretical values but noise gradually increases as ε rises from 0.018 rad to 0.07 rad. To intuitively illustrate the variation, SNRs are calculated and equal to 17.81 dB, 13.91 dB, and 10.97 dB for $\varepsilon = 0.018, 0.035$, and 0.07 rad respectively; these fall within theoretical predictions. Compared to previous weak measurement methods, the proposed method ensures that weak measurements can suppress technical noise and amplify weak signals under significant attenuation of light intensity. Furthermore, the precision of about 10^{-8} rad could potentially be achieved by using current equipment while setting the post-selection angle at 10^{-4} rad. The signal light intensity feeding into the VOA is measured at 3 dBm. Consequently, the signal light intensity without attenuation is −31.9 dBm when $\varepsilon = 0.018$ rad. Experimental results indicate that the system can achieve precise phase characterization even with a light intensity attenuation of 48.1 dB, which means that it may be suitable for long-distance and high-loss sensing scenarios. In subsequent implementation, the proposed method is utilized for detecting a 3-bit binary coded communication signal following significant light intensity attenuation, where the first, second, and third bits modulate the initial phase, frequency, and amplitude of the sinusoidal signal, respectively; and the modulated principle is shown in Fig. 1(b). Experimental results presented in Fig. 3(c) demonstrate that eight cases of the jointly modulated sinusoidal signals can be clearly distinguished, thereby enabling effective extraction of encoded information.

In conclusion, we have proposed and experimentally demonstrated an enhanced long-distance weak signal transmission method via weak measurement. The approach can extract weak signals through light intensity detection and has the capability of monitoring time-varying parameters at the GHz level. With the intensity compensation on the detection value of two post-selected measurement paths, the stringent requirement for symmetry can also be eliminated. By incorporating heterodyne detection, the proposed method enables precise characterization of weak phase signals even when light intensity is attenuated by 48.1 dB, potentially achieving a precision of approximately 10^{-8} rad. In practical applications, the time-varying phase is unknown and stochastic, which may exceed the linear dynamic range of the system. Current research on adjusting sensitivity, precision, and linear dynamic range can be applied in the proposed approach.[21,32,39,40] For example, inserting a pair of symmetrical reference phases can achieve the adjustable sensitivity and linear dynamic range; improving Fisher information further suppresses systematic errors related to coupling strength. The approach may serve as a potential solution in long-distance weak signal detection and extraction, contributing to O-ICAS.

Acknowledgements. This work was supported by the National Natural Science Foundation of China

(Grant No. 62471289), the Natural Science Foundation of Shanghai (Grant No. 24ZR1432900), the Innovation Program for Quantum Science and Technology (Grant No. 2021ZD0300703), and Shanghai Municipal Science and Technology Major Project (Grant No. 2019SHZDZX01).

References

[1] Messer H, Zinevich A, and Alpert P 2006 *Science* **312** 713
[2] Schedl D C, Kurmi I, and Bimber O 2021 *Sci. Robot.* **6** eabg1188
[3] Huang Q Y, Chen H X, and Zhang Q 2020 *IEEE Netw.* **34** 191
[4] Wang J, Varshney N, Gentile C, Blandino S, Chuang J, and Golmie N 2022 *IEEE Internet Things J.* **9** 23416
[5] Li X Y, Gong Y, Huang K B, and Niu Z S 2023 *IEEE Wireless Commun.* **30** 32
[6] Saad W, Bennis M, and Chen M 2019 *IEEE Netw.* **34** 134
[7] Liu F, Cui Y, Masouros C, Xu J, Han T X, Eldar Y C, and Buzzi S 2022 *IEEE J. Sel. Areas Commun.* **40** 1728
[8] Zheng K, Zheng Q, Yang H J, Zhao L, Hou L, and Chatzimisios P 2015 *IEEE Commun. Mag.* **53** 72
[9] Yuan W J, Liu F, Masouros C, Yuan J H, Ng D, and Gonzalez-Prelcic N 2021 *IEEE Trans. Wireless Commun.* **20** 1442
[10] Chen J P, Zhang C, Liu Y, Jiang C, Zhao D F, Zhang W J, Chen F, Li H, You L, Wang Z, Chen Y, Wang X, Zhang Q, and Pan J W 2022 *Phys. Rev. Lett.* **128** 180502
[11] Xu Y H, Wang T, Huang P, and Zeng G H 2024 *Research* **7** 0416
[12] He H J, Jiang L, Pan Y, Yi A L, Zou X H, Pan W, Willner A, Fan X Y, He Z Y, and Yan L S 2023 *Light Sci. Appl.* **12** 25
[13] He Z Y and Liu Q W 2021 *J. Lightwave Technol.* **39** 3671
[14] Li J X, Kim T, Lapusta N, Biondi E, and Zhan Z W 2023 *Nature* **620** 800
[15] Liu S S, Tian Y, Zhang Y, Lu Z G, Wang X Y, and Li Y M 2024 *Optica* **11** 1762
[16] Wei Z Q, Qu H Y, Jiang W J, Han K F, Wu H C, and Feng Z Y 2023 *IEEE. Trans. Green. Commun. Networking* **7** 401
[17] Laudenbach F, Pacher C, Fung C H F, Poppe A, Peev M, Schrenk B, Hentschel M, Walther P, and Hubel H 2018 *Adv. Quantum Technol.* **1** 1800011
[18] Gorshkov B G, Alekseev A E, Taranov M A, Simikin D E, Potapov V T, and Ilinskiy D A 2022 *Opt. Appl.* **61** 8308
[19] Horiguchi T and Tateda M 1989 *Opt. Lett.* **14** 408
[20] Xie C L, Guo Y, Wang Y J, Huang D, and Zhang L 2018 *Chin. Phys. Lett.* **35** 090302
[21] Zhang M C, Zhang J, Su W B, Yang X Y, Wu C W, Xie Y, Wu W, and Chen P X 2023 *Chin. Phys. Lett.* **40** 040301
[22] Xu L and Zhang L J 2024 *Prog. Quant. Electron* **96** 100518
[23] Shang W M, Zhou J, Meng H X, and Chen J L 2020 *Chin. Phys. Lett.* **37** 050302
[24] Martinez-Rincon J, Mullarkey C A, Viza G I, Liu W T, and Howell J C 2017 *Opt. Lett.* **42** 2479
[25] Brunner N and Simon C 2010 *Phys. Rev. Lett.* **105** 010405
[26] Wu Y P, Liu S Q, Chen S Z, Luo H L, and Wen S C 2022 *Opt. Lett.* **47** 846
[27] Strubi G and Bruder C 2013 *Phys. Rev. Lett.* **110** 083605
[28] Martinez-Rincon J, Chen Z K, and Howell J C 2017 *Phys. Rev. A* **95** 063804
[29] Martinez-Rincon J, Liu W T, Viza G I, and Howell J C 2016 *Phys. Rev. Lett.* **116** 100803
[30] Zhang Z H, Chen G, Xu X Y, Tang J S, Zhang W H, Han Y J, Li C F, and Guo G C 2016 *Phys. Rev. A* **94** 053843
[31] Huang J Z, Li Y J, Fang C, Li H J, and Zeng G H 2019 *Phys. Rev. A* **100** 012109
[32] Song Q, Li H J, Huang J Z, Xiao T L, Tan X R, Xia B K, and Zeng G H 2022 *Phys. Rev. Appl.* **18** 044031
[33] Shi C H, Song Q, Li H J, Tan X R, Luo Z Y, Huang J Z, and Zeng G H 2024 *Appl. Phys. Lett.* **124** 120001
[34] Qiu X D, Xie L G, Liu X, Luo L, Li Z X, Zhang Z Y, and Du J L 2017 *Appl. Phys. Lett.* **100** 071105
[35] Zhang L J, Datta A, and Walmsley I A 2015 *Phys. Rev. Lett.* **114** 210801
[36] Song Q, Li H J, Huang J Z, Huang P, Tan X R, Tao Y, Shi C H, and Zeng G H 2023 *Commun. Phys.* **6** 370
[37] Jozsa R 2007 *Phys. Rev. A* **76** 044103
[38] Dressel J, Malik M, Miatto F M, Jordan A N, and Boyd R W 2014 *Rev. Mod. Phys.* **86** 307
[39] Zhang M C, Zhang J, Wu C W, Xie Y, Chen T, Wu W, and Chen P X 2023 *Phys. Rev. A* **107** 042601
[40] Li H J, Wang G L, Xia B K, Song Q, Huang J Z, and Zeng G H 2021 *J. Phys. B At. Mol. Opt.* **54** 215503